IEEE Access
Multidisciplinary | Rapid Review | Open Access Journal

Received June 18, 2020, accepted June 23, 2020, date of publication June 30, 2020, date of current version July 20, 2020.

*Digital Object Identifier 10.1109/ACCESS.2020.3006076*

# Design of Smartwatch Integrated Antenna With Polarization Diversity

**BUYUN WANG[1] AND SEN YAN[1,2], (Member, IEEE)**
[1]School of Information and Communications Engineering, Xi'an Jiaotong University, Xi'an 710049, China
[2]Shenzhen Research School, Xi'an Jiaotong University, Shenzhen 518057, China

Corresponding author: Sen Yan (sen.yan@xjtu.edu.cn)

This work was supported in part by the National Natural Science Foundation of China under Grant 61901351, in part by the Technology Program of Shenzhen under Grant JCYJ20180306170841629, and in part by the Outstanding Scientific and Technological Programs Foundation for the Returned Overseas Chinese Scholars of Shaanxi province under Grant 2018014.

**ABSTRACT** A design of smartwatch integrated antenna with polarization diversity is proposed. An annular ring is integrated in the framework of smartwatch, and excited by two ports. One port is fed by a coplanar waveguide (CPW) line loaded with a T-shaped matching network, and the other is fed by a coplanar strip line (CPS). The overall model of the proposed antenna has a cylindrical shape with 38 mm diameter and 7.5 mm thickness. A metallic plate is located at the backside of the antenna to mimic the shell of smartwatch. The prototype is fabricated and measured, and the measured results agree well with the numerical ones. The two ports have orthometric radiation patterns and can cover the 2.4 GHz wireless local area network (WLAN) band. The gain of the antenna is higher than 3.2 dBi in free space. The proposed antenna is also analyzed with a cubic tissue model and a wrist model in different distances between the proposed antenna and human models. The performances on body scenarios are also acceptable. The values of specific absorption rate (SAR) in the cubic tissue model and wrist model are below the limitations set by both the Federal Communication Commission (FCC) and the European Telecommunication Standards Institute (ETSI). Envelope correlation coefficient (ECC) shows proposed antenna can be used in multiple input multiple output (MIMO) applications. The influence of battery and printed circuits board assembly (PCBA) on S parameters is obvious, and gain and radiation efficiency are not much affected.

**INDEX TERMS** Wireless body area network (WBAN), wearable antenna, smartwatch integrated antenna, polarization diversity, cubic tissue model, wrist model, specific absorption rate (SAR), Envelope correlation coefficient (ECC).

## I. INTRODUCTION

Wireless body area network (WBAN) is a small communication network attached to the body. In recent years, it has attracted increasing attention because it can play an important part in medical detection, fitness training, health care and emergency rescue [1]. As one of the critical components in wearable smart devices, wearable antenna can transmit the microwave signals in the wireless communication systems between the devices and sensors [2]. Smartwatch is one of the most favorite wearable smart devices. It can inform their users of their current location, current time, the steps and the distance they have walked, the prospective weather situation, their physiology parameters, and etc. Normally, most of these data need to be synchronized with other smart devices, e.g. smartphones and personal computers, for deep analysis and long-term storage [3]. However, due to the size of the normal devices and the crowded arrangement of the inner components, antenna design is a challenge work in smartwatches, especially considering the strong coupling between the antenna and the human body. One of the popular antenna types for smartwatch was planar Inverted-F antenna (PIFA) [4]–[6], which was easy to cover a single band, usually the 2.4 GHz WLAN band, with a compact size. To realize multifunction, several modified multi-band PIFAs or monopole antennas were also proposed [7]–[12]. However, these structures could hardly be integrated with the framework of smartwatch and thus, were not suitable for the designs with totally metallic frame. Recently, the antennas integrated in the structures of smartwatches were proposed and studied, such as several antenna designs with metallic frame of smartwatches [13]–[17]. Although these designs

The associate editor coordinating the review of this manuscript and approving it for publication was Weiren Zhu.


This work is licensed under a Creative Commons Attribution 4.0 License. For more information, see https://creativecommons.org/licenses/by/4.0/

had some special advantages, none of them used diversity technology. Besides, some designs proposed the solutions of locating antennas and feeding ports on watch straps [18]–[20]. However, these designs were completely ingenious but not very practical due to the various deformations when worn on the user's wrist and also the unrealizable feeding connection between the antennas on the belt and the RF circuits in the body of the watches.

Antenna diversity technologies can significantly improve the performance of wireless communication systems in multi-reflection environments. Several scholars proposed dual-port antennas with polarization diversity and high port isolation [21]–[26]. However, due to their topologies and sizes, these designs could hardly be applied to real smartwatch and body scenarios. Most of these designs did not consider the integration between antenna and smartwatch, and the coupling between antenna and human tissue.

We propose a design of smartwatch integrated antenna with polarization diversity for 2.4 GHz WLAN applications. The proposed antenna has a simple structure because smart watch antenna is generally limited by its structure, and the proposed antenna compared to the existing antennas realizes diversity technology, which has not been realized in the previous smart watch antenna. The initial design idea is that two ports excite the odd and even modes of a ring resonator respectively, which has been presented in our previous work [27]. In this paper, the complete design and structure, operating mechanism, experimental and measured results, SAR results, ECC, and influence of battery and PCBA are fully analyzed which were not shown in [27], together with the measured results in free space and on the human body models (including cubic tissue model and wrist model). The final topology of the proposed antenna has a cylindrical shape. The diameter of the proposed antenna is 38 mm, and the height is 7.5 mm referring to the general height of the smart watch, which makes it easy to be integrated in the frame of normal smartwatch. The commercial simulation solver HFSS and CST are used in the design and calculation.

## II. CONFIGURATION AND STRUCTURE

In this chapter, the configurations of the simulation model in free space, with the cubic tissue model, and with wrist model are proposed.

### A. ANTENNA DESIGN

Fig. 1 shows the geometry of the proposed antenna. The overall model has three layers. The top layer and the bottom layer are both FR-4 circuit boards ($\varepsilon_r = 4.3$, $\tan\delta = 0.02$), and the antenna is located on the surface of the top FR-4 board. The middle layer is a foam board ($\varepsilon_r = 1.1$) which is used to pad the antenna up. All the values of the geometry parameters are shown in Fig. 1 and TABLE 1.

A split ring resonator plays the main body of the antenna [21], [27]. As shown in Fig. 1 (a), the antenna is composed of a T-shaped line and two metallic arcs. The T-shaped line for impedance matching is the extension of the inner signal

**TABLE 1. Geometry parameters of the proposed antenna.**

| Geometry Parameter | Length (mm) | Geometry Parameter | Length (mm) |
|---|---|---|---|
| R | 19 | h | 5.9 |
| r | 17 | $h_1$ | 0.8 |
| $r_1$ | 15 | $h_3$ | 0.5 |
| $w_0$ | 1.3 | $l_1$ | 5.6 |
| $w_1$ | 4 | $l_2$ | 17 |
| $w_2$ | 1.1 | $w_3$ | 1.5 |
| $w_4$ | 1 | | |

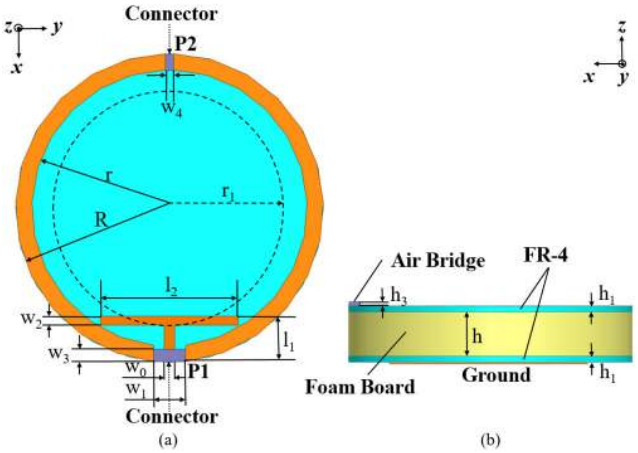


**FIGURE 1. Geometry of proposed antenna. (a)Top view. (b)Side view.**

line of the feeding CPW (port 1). The two metallic arcs are connected to the two outer ground planes of the CPW, and the electric length of one arc is about a half wavelength at 2.4 GHz. There is an air bridge wire across the port 1, which connects the two outer ground planes of the CPW together, shown in Fig. 1 (b), thus the annular ring is constructed. The annular ring connected to a CPS is excited by the port 2 at the other side of the antenna. A circular metallic shell is located under the bottom FR-4 board to mimic the backed shell of smartwatch, called 'Ground'. The design procedure: choosing appropriate values of 'h', 'R', 'r', '$r_1$' can realize impedance matching of port 2. Then, designing the geometry of T-shaped line can realize impedance matching of port 1.

Fig. 2 shows the simulated current distributions at 2.4 GHz. Port 1 is a CPW port. It is a common mode feed port which can excite the even mode. When port 1 is excited, the currents are distributed on the side metallic arcs with the current node at port 2 position, as shown in Fig. 2 (a), which will bring a low coupling between the two ports. Actually, the symmetric structure is the main reason for the good isolation. The current excited by port 1 is along the $x$- axis. Port 2 is a CPS port. It is a differential mode feed port which can excite the odd mode. When port 2 is excited, the currents are distributed on the side metallic arcs with the current node at the middle position of the metallic arcs, as shown in Fig. 2 (b). The current excited by port 2 is along the $y$- axis. Thus, the current on both the $x$- and the $y$- axis could be expected of this design from different feeding ports at 2.4 GHz, so the proposed antenna can realize orthometric radiation patterns in far field. Fig. 3 and Fig. 4 show the fabricated antenna

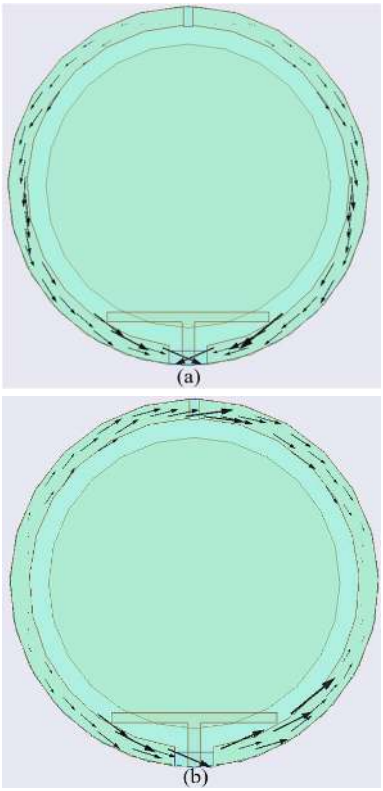


**FIGURE 2.** Simulated current distributions. (a) When P1 excited. (b) When P2 excited.

**FIGURE 3.** The fabricated antenna.

and the experimental environment in the microwave chamber for measurement. Two FR-4 boards are fabricated as printed circuits boards (PCB).

### B. STRUCTURE WITH CUBIC TISSUE MODEL

Fig.5 shows the structure of the proposed antenna with the cubic tissue model. The cubic tissue model is constructed to three cuboid layers. They are skin, fat and muscle from top to bottom, respectively [28]. The thickness is 2 mm of skin, 5 mm of fat, and 20 mm of muscle. The length of the cuboid is 150 mm. These geometry parameters are to mimic the human body tissue. The parameters of each tissues are set from the material library in CST.

### C. STRUCTURE WITH WRIST MODEL

Fig. 6 shows the structure of the proposed antenna with the wrist model. The wrist model is constructed to four cylindroid

**FIGURE 4.** The antenna in microwave chamber for measurement.

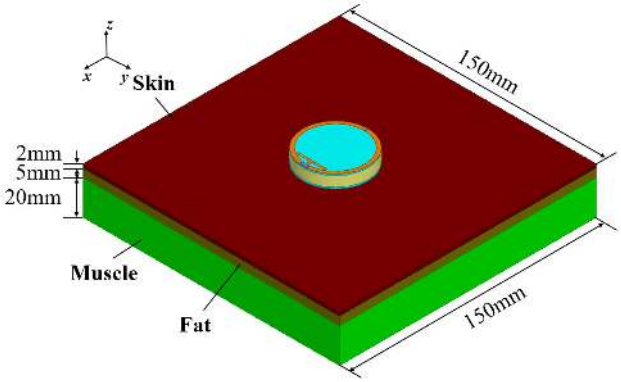


**FIGURE 5.** Geometry with the cubic tissue model.

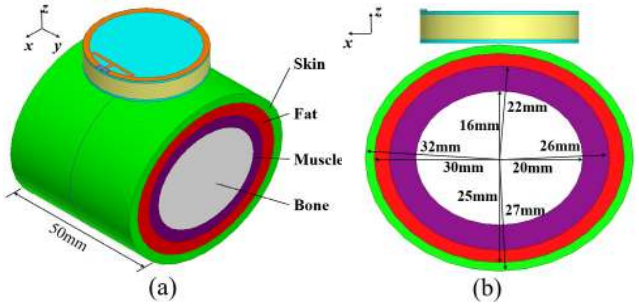


**FIGURE 6.** Geometry with the wrist model. (a) Full view. (b) Side view.

layers which are skin, fat, muscle and bone from its out to core [18]. The material parameters of the human tissue model are shown in TABLE 2 at 2.4 GHz. The distance between the 'Ground' and the human tissue model is written as 'd'(mm).

## III. PERFORMANCES AND RESULTS

The proposed antenna is fabricated and measured. The results of simulation and measurement are analyzed in free space, and with the cubic tissue model and wrist model.

### A. S PARAMETERS

The S parameters in free space are shown in Fig. 7 (a). In free space, port 1 operating band ($S_{11} < -10$ dB, VSWL $< 2$) is from 1.89 GHz to 2.93 GHz in simulation, and from 1.89 GHz

**TABLE 2. Material parameters of body model (2.4 GHz).**

| Human Tissue | $\varepsilon_r$ | $\sigma$ (S/m) | tan $\delta$ |
|---|---|---|---|
| Skin | 38.06 | 1.44 | 0.28 |
| Fat | 5.29 | 0.11 | 0.15 |
| Muscle | 52.79 | 1.71 | 0.24 |
| Bone | 18.49 | 0.82 | 0.25 |

to 2.62 GHz in measurement. The overlapped bandwidth in free space is 1040 MHz in simulation, and 730 MHz in measurement, which can cover the band for 2.4 GHz WLAN applications. Port 2 operating band is from 2.33 GHz to 2.50 GHz in simulation, and from 2.31 GHz to 2.53 GHz in measurement. The overlapped bandwidth in free space is 170 MHz in simulation, and 220 MHz in measurement, which can also cover the band for 2.4 GHz WLAN applications. In the band range of 2.4 GHz – 2.5 GHz, the isolation between the two ports ($S_{21}$) is lower than −13 dB in free space.

Fig. 7 (b) shows the S parameters with the cubic tissue model when d is 0.5mm and 2mm. Fig. 7 (c) shows the S parameters with the wrist model when d is 0.5mm and 2mm, and especially the measurement results. The operating bands of both ports move to lower frequency because of the influence of human tissue, but they still cover 2.4 GHz WLAN bandwidth. The values of port isolation $S_{21}$ is lower than −12 dB on body scenario on the band range of 2.4 GHz to 2.5 GHz.

TABLE 3, TABLE 4 and TABLE 5 list all the values of operating band and bandwidth when antenna is in those three situations. When the antenna is put on the cubic model, its lowest bandwidth is 260 MHz when d is 0.5mm. When the antenna is put on the wrist model, the lowest bandwidth is 500 MHz when d is 2mm. These two lowest bandwidths are both sufficient for smartwatch antenna at 2.4 GHz WLAN. As for comparison between simulated results and measurement, there is little difference of the operating band between the simulation and measurement both in free space and on the wrist model, as shown in TABLE 3 and TABLE 5. The simulated results and measurements can cover the 2.4 GHz WLAN band. TABLE 6 shows that operating band is not much affected by the hand in measurement, because the ring is about 8 mm away from the hand, which reduces the impact.

### B. RADIATION PERFORMANCES

The simulated and measured radiation patterns of the proposed antenna in free space are shown in Fig. 8. The results are tested at 2.4 GHz. When one port is fed and tested, the other port is connected with a matched load. The radiation patterns between simulated results and measurement are close in Fig. 8. The results reveal that the realized gain of port 1 is 3.7 dBi in simulation and 3.2 dBi in measurement, while the realized gain of port 2 is 4.6 dBi in simulation and 4.7 dBi in measurement. It's close between the simulated and measured realized gain. Thus, the results of radiation pattern and realized gain between simulation and measurement are close. The cross-polarizations are below −10 dB for both the two ports. Furthermore, the radiations of the two ports have orthometric polarizations, which accords with the current

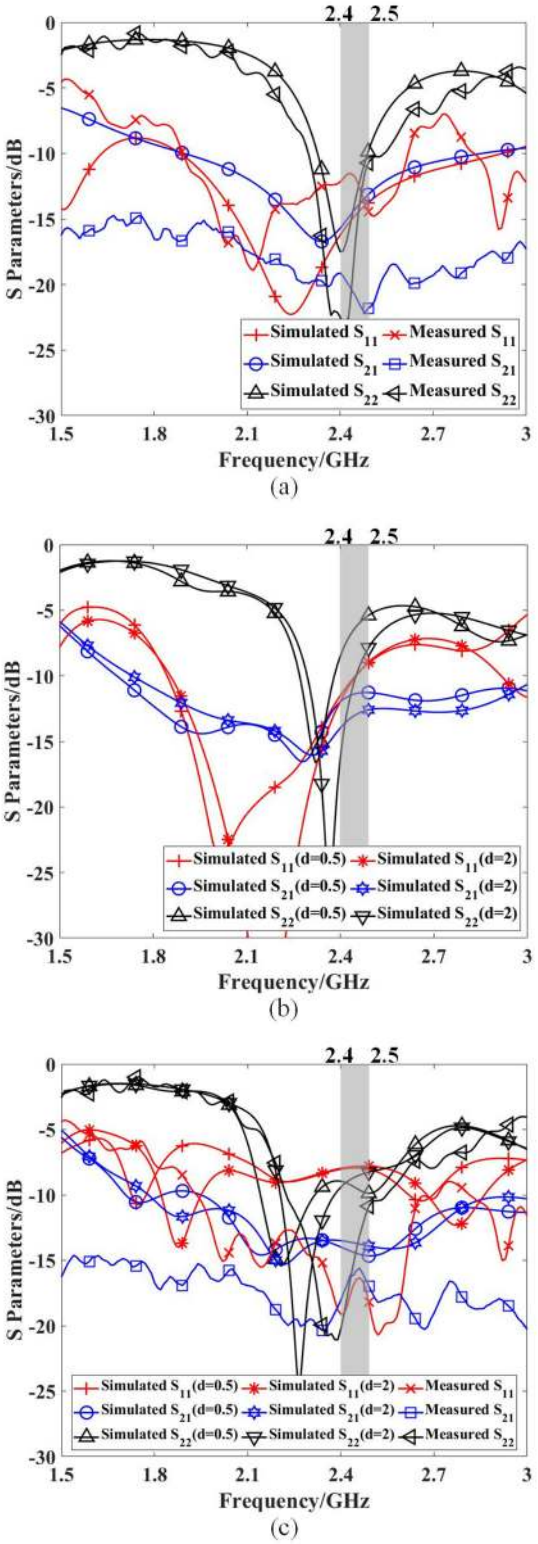


**FIGURE 7. S parameters (a) in free space. (b) with cubic tissue model. (c) with wrist model. d (mm) is the distance between the antenna and the human tissue model. The same color represents the same S parameter: red is $S_{11}$; blue is $S_{21}$; black is $S_{22}$. The gray zone is the frequency band from 2.4 GHz to 2.5 GHz.**

**TABLE 3. Operating band (−10dB) in free space.**

| Port | Operating Band (GHz) | Bandwidth (MHz) |
|---|---|---|
| Simulated Port 1 | 1.89 – 2.93 | 1040 |
| Simulated Port 2 | 2.33 – 2.50 | 170 |
| Measured Port 1 | 1.89 – 2.62 | 730 |
| Measured Port 2 | 2.31 – 2.53 | 220 |

**TABLE 4. Operating band (−6dB) with cubic tissue model.**

| d | Port | Operating Band (GHz) | Bandwidth (MHz) |
|---|---|---|---|
| 2mm | Simulated Port 1 | 1.68 – 2.62 | 940 |
| | Simulated Port 2 | 2.24 – 2.54 | 300 |
| 0.5mm | Simulated Port 1 | 1.73 – 2.86 | 1130 |
| | Simulated Port 2 | 2.22 – 2.48 | 260 |

**TABLE 5. Operating band (−6dB) with wrist model.**

| d | Port | Operating Band (GHz) | Bandwidth (MHz) |
|---|---|---|---|
| 2mm | Simulated P1 | 1.72 – 3.22 | 1500 |
| | Simulated P2 | 2.18 – 2.68 | 500 |
| 0.5mm | Simulated P1 | 1.92 – 3.15 | 1230 |
| | Simulated P2 | 2.11 – 2.63 | 520 |
| On Real Wrist | Measured P1 | 1.79 – 3.13 | 1340 |
| | Measured P2 | 2.18 – 2.85 | 670 |

**TABLE 6. Operating band (−10dB) in measurement.**

| Environment | Port | $S_{ii}$ at 2.4 GHz | Operating Band (GHz) | Bandwidth (MHz) |
|---|---|---|---|---|
| Free Space | P1 | -13 dB | 1.89 – 2.62 | 730 |
| | P2 | -23 dB | 2.31 – 2.53 | 220 |
| Real Wrist | P1 | -18 dB | 1.96 – 2.65 | 690 |
| | P2 | -21 dB | 2.25 – 2.51 | 260 |

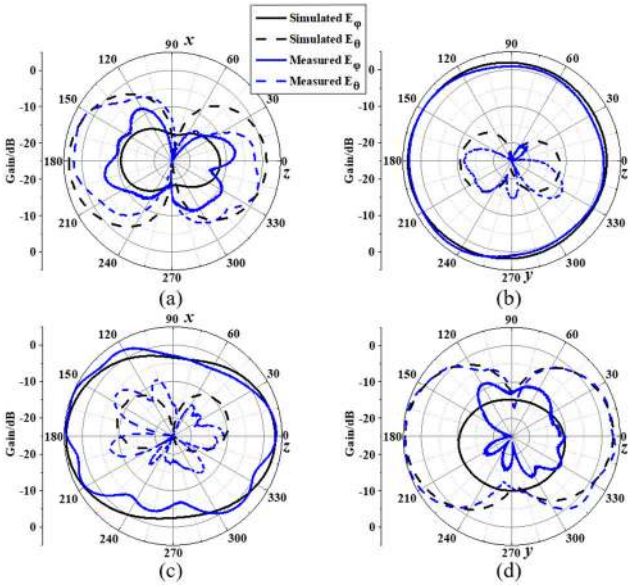


**FIGURE 8. Radiation patterns in free space at 2.4 GHz. (a) xz-plane when P1 is excited; (b) yz-plane when P1 is excited; (c) xz-plane when P2 is excited; (d) yz-plane when P2 is excited.**

**TABLE 7. Values of peak gain and radiation efficiency in free space and with human body model.**

| Environment | Situation | Peak Gain (dBi) | | Radiation Efficiency | |
|---|---|---|---|---|---|
| | | Port 1 | Port2 | Port 1 | Port 2 |
| Free Space | Simulated | 3.7 | 4.6 | 97% | 98% |
| | Measured | 3.2 | 4.7 | 88% | 81% |
| Cubic Tissue Model | d=0.5 | 2.2 | 3.7 | 32% | 44% |
| | d=2 | 3.9 | 4.9 | 52% | 57% |
| Wrist Model | d=0.5 | 4.2 | 4.0 | 75% | 62% |
| | d=2 | 4.7 | 4.9 | 77% | 71% |

distributions in Fig. 2. The values of measured radiation efficiency are higher than 80%, which is a bit lower than the simulated one, shown in TABLE 7. It is caused by processing loss and cable loss.

Fig. 9 shows the radiation patterns with the cubic tissue model and wrist model when d is 2 mm 0.5 mm at 2.4 GHz. The peak gain and efficiency of the same port with wrist model is higher than it with cubic tissue model when d is same. When d reduces from 2 mm to 0.5 mm, the gain and efficiency will be lower because the closer between antenna and human body, the more power human body absorbs. When the proposed antenna is on cubic tissue model, the values of peak gain and radiation efficiency are higher than 2.2 dBi and 32%, respectively, which are sufficient for smartwatch applications. When the antenna is put on wrist model, the values of peak gain and radiation efficiency are even higher than 4 dBi and 62%.

### C. SAR ANALYSES

The SAR is a value to represents the RF power-absorption rate by a unit mass of tissue within a unit time. The density ($\rho$) of the human tissue is 1000 kg/m$^3$. According to the limitation that the maximum of equivalent isotropically radiated power (EIRP) is 20 dBm for 2.4 GHz band [29] and the peak gain which is more than 3 dBi of proposed antenna in foregoing results, we set the input power on both two ports of the proposed antenna to 17 dBm (50 mW). Measurement of SAR value is complicated. Our laboratory does not support it, but our fellows had a previous work to verify the accuracy and reliability of SAR value simulation [30]. Thus, we use simulation package HFSS and CST to calculate and analyze SAR results.

Fig. 10 shows the 10-g SAR and 1-g SAR distribution in *xz*-plane at 2.4 GHz with cubic tissue model when d is 2 mm. The peak SAR value appears in the center of the muscle layer in the cubic tissue model. The 10-g SAR peak value is about 0.6980 W/kg of port 1 and 0.7698 W/kg of port 2. The 1-g SAR peak value is about 0.9561 W/kg of port 1 and 1.0569 W/kg of port 2.

Fig. 11 shows the 10-g SAR and 1-g SAR distribution in *xz*-plane at 2.4 GHz with wrist model when d is 2 mm. The peak SAR value also appears in the center of the muscle layer

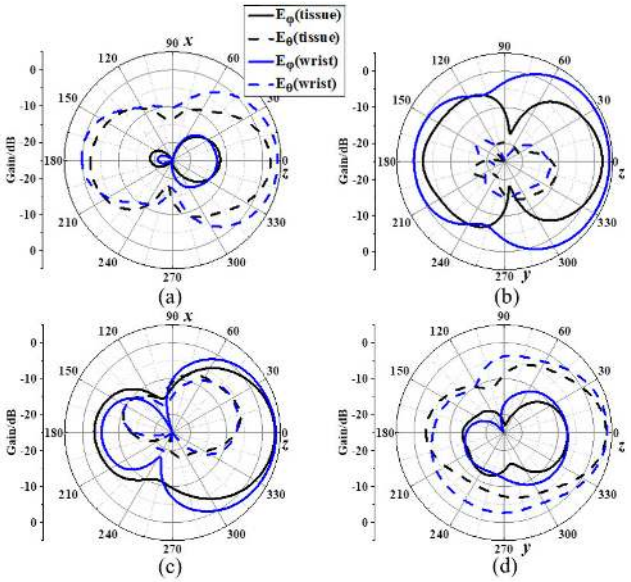


**FIGURE 9.** Radiation patterns on body scenarios at 2.4 GHz. (a) xz-plane when P1 is excited; (b) yz-plane when P1 is excited; (c) xz-plane when P2 is excited; (d) yz-plane when P2 is excited.

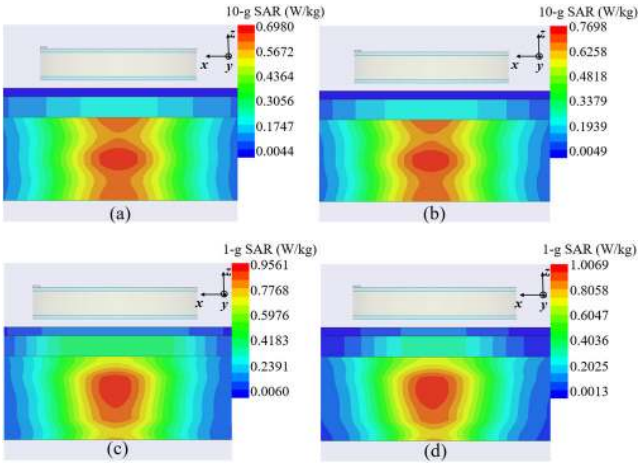


**FIGURE 10.** SAR distributions with cubic tissue model in HFSS when d is 2mm. (a)10-g SAR of port 1. (b)10-g SAR of port 2. (c) 1-g SAR of port 1. (d) 1-g SAR of port 2.

in the wrist model. The SAR values with cubic tissue model and wrist model when d is 0.5mm are also analyzed. All the specific values are shown in TABLE 7 and TABLE 8.

TABLE 8 lists SAR values with cubic tissue model and wrist model when d is 2 mm in both two software, and TABLE 9 lists SAR values when d is 0.5 mm. These two tables show the results calculated by HFSS and CST are similar. According to these two tables, when d reduces from 2 mm to 0.5 mm, the 10-g SAR value and 1-g SAR value will be higher, it is also because the closer between antenna and human body. The limitations about SAR values set by Federal Communication Commission (FCC) and European Telecommunication Standards Institute (ETSI) [31] are also listed in the two tables. According to the regulations, all the SAR values of proposed antenna are less than the corresponding SAR limitations set by both the FCC and ETSI. It means

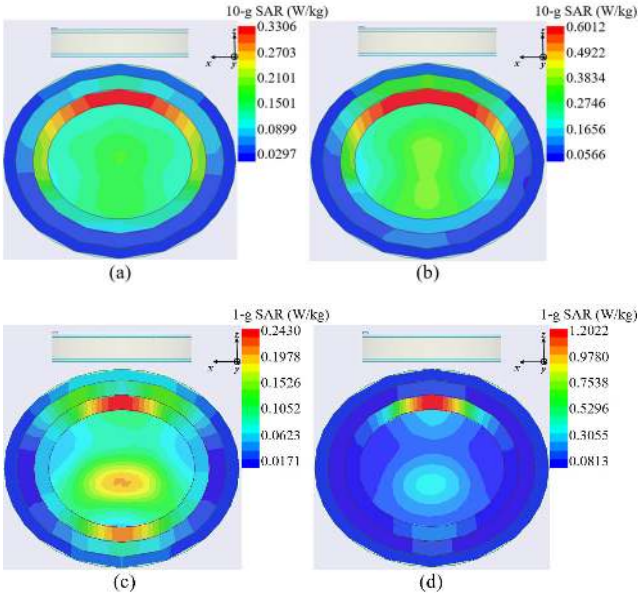


**FIGURE 11.** SAR distributions with wrist model in HFSS when d is 2mm. (a)10-g SAR of port 1. (b)10-g SAR of port 2. (c) 1-g SAR of port 1. (d) 1-g SAR of port 2.

**TABLE 8.** SAR values when d is 2 mm and limitations.

| Limitations & Proposed Antenna Port | Simulation Software | 10-g SAR (W/kg) | 1-g SAR (W/kg) |
|---|---|---|---|
| FCC limitation | / | 4.0 | 1.6 |
| ETSI limitation | / | 2.0 | 1.6 |
| Port 1 with cubic model | HFSS | 0.6980 | 0.9561 |
| Port 2 with cubic model | HFSS | 0.7698 | 1.0069 |
| Port 1 with wrist model | HFSS | 0.3306 | 0.2430 |
| Port 2 with wrist model | HFSS | 0.6012 | 1.2022 |
| Port 1 with cubic model | CST | 0.6254 | 0.5609 |
| Port 2 with cubic model | CST | 0.5692 | 0.7984 |
| Port 1 with wrist model | CST | 0.3191 | 0.3442 |
| Port 2 with wrist model | CST | 0.6607 | 1.2514 |

that the radiation effect on human body created by proposed antenna can be ignored. The proposed antenna will not make terrible effect on human health.

### D. COMPARISON

TABLE 9 shows the comparison between the proposed antenna and other designs of smartwatch antennas in literatures. In size and structure, the planar dimension of the proposed antenna (diameter is 0.3 λ) is smaller than some of designs in references in TABLE 10. The height of proposed antenna (7.5 mm) refers to the size of the general smart watch, unlike antennas in [6], [8], [10], [11] whose heights were not suitable for a watch. In performance, the bandwidth, gain and radiation efficiency of the proposed antenna with hand

**TABLE 9. SAR values when d is 0.5 mm and limitations.**

| Limitation & Proposed Antenna Port | Simulation Software | 10-g SAR (W/kg) | 1-g SAR (W/kg) |
|---|---|---|---|
| FCC limitation | / | 4.0 | 1.6 |
| ETSI limitation | / | 2.0 | 1.6 |
| Port 1 with cubic model | HFSS | 0.8300 | 1.4850 |
| Port 2 with cubic model | HFSS | 0.5728 | 0.5837 |
| Port 1 with wrist model | HFSS | 0.2221 | 0.2922 |
| Port 2 with wrist model | HFSS | 0.4444 | 1.5867 |
| Port 1 with cubic model | CST | 0.7245 | 1.3942 |
| Port 2 with cubic model | CST | 0.4345 | 0.4104 |
| Port 1 with wrist model | CST | 0.2894 | 0.3547 |
| Port 2 with wrist model | CST | 0.4255 | 1.5393 |

**TABLE 10. Comparison between proposed antenna and other smartwatch antennas in references. 'λ' means the wavelength corresponding to the lowest operating frequency. '$\varphi$' means diameter.**

| Ref. | Dimensions ($\lambda^3$) | Bandwidth at 2.4 GHz WLAN band on hand model (MHz) | Operating frequency (GHz) |
|---|---|---|---|
| [6] | 0.29×0.25×0.004 | Not given | 2.4/3.5/5.2 |
| [7] | 0.21×0.21×0.028 | Not given | 1.57/1.94/2.4 |
| [8] | 0.25×0.25×0.008 | 160 | 2.4/5.2 |
| [9] | 0.30×0.21×0.03 | Not given | 1.57/1.8/2.4 |
| [10] | 0.4×0.27×0.009 | Not given | 2.4/5.2 |
| [11] | 0.27×0.27×0.003 | Not given | 2.4/3.5/5.0 |
| [13] | 0.35(φ)×0.35×0.08 | 95 | 2.4 |
| [15] | 0.42×0.33×0.042 | 400 | 2.4 |
| [16] | 0.3×0.3×0.042 | Not given | 1.57/2.4/3.5 |
| **proposed** | **0.3(φ)×0.3×0.058** | **500** | **2.4** |

| Ref. | Gain at 2.4 GHz on hand model (dBi) | Radiation efficiency on hand model | Polarization diversity |
|---|---|---|---|
| [6] | Not given | Not given | No |
| [7] | Not given | Not given | No |
| [8] | Not given | Not given | No |
| [9] | Not given | Not given | No |
| [10] | Not given | Not given | No |
| [11] | Not given | Not given | No |
| [13] | 2.79 | 57% | No |
| [15] | -0.89 | 26% | No |
| [16] | Not given | Not given | No |
| **proposed** | **4.0** | **62%** | **Yes** |

model are also the highest one, 500 MHz, 4.0 dBi and 62%, respectively. Most importantly, the proposed antenna is with polarization diversity which was not realized in the existing smart watch antenna, and it can be well integrated in the framework of smartwatch because of its annular shape.

## IV. DISCUSSION

This chapter calculates the ECC to determine whether the proposed antenna can be used in MIMO applications, and adds the battery and PCBA into the inner structure to analyze the influence of them.

**TABLE 11. ECC at 2.4 GHz.**

| Situation | $\rho_{12}$ by simulated S parameters | $\rho_{12}$ by measured S parameters | Measured $\rho_{12}$ in far field |
|---|---|---|---|
| Free Space | $1.126\times10^{-3}$ | $7.794\times10^{-4}$ | $1.109\times10^{-2}$ |
| Cubic Tissue (d=2) | $3.519\times10^{-3}$ | / | / |
| Cubic Tissue (d=0.5) | $1.368\times10^{-2}$ | / | / |
| Wrist (d=2) | $1.252\times10^{-2}$ | / | / |
| Wrist (d=0.5) | $1.162\times10^{-2}$ | / | / |
| Real wrist | / | $3.738\times10^{-3}$ | / |

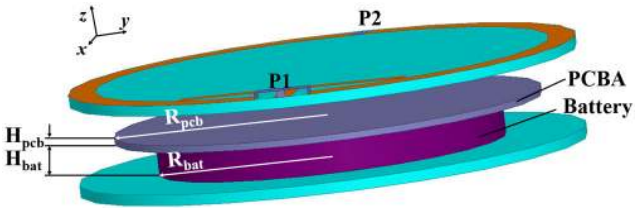


**FIGURE 12. Antenna model after adding the battery and PCBA.**

**TABLE 12. Gain and Efficiency with battery and PCBA at 2.4 GHz. $R_{bat}$, $R_{pcb}$, $H_{bat}$ are in millimeters. $H_{pcb}$ = 0.5mm.**

| $R_{bat}$ | $R_{pcb}$ | $H_{bat}$ | Gain (P1) | Gain (P2) | Radiation efficiency (P1) | Radiation efficiency (P2) |
|---|---|---|---|---|---|---|
| 13 | 16 | 2.5 | 3.2dBi | 4.2dBi | 95.6% | 94.8% |
| **16** | 16 | 2.5 | 3.1dBi | 4.2dBi | 95.5% | 94.8% |
| 13 | **19** | 2.5 | 3.0dBi | 4.1dBi | 90.4% | 88.9% |
| 13 | 16 | **3.0** | 3.2dBi | 4.2dBi | 95.6% | 94.8% |

### A. ECC

ECC is a parameter to evaluate whether the antenna can be used in MIMO applications. It can be calculated by S parameters [32] or by this formula in far field [33]:

$$\rho_{12} = \frac{|\iint_{4\pi} \vec{F}_1(\theta,\varphi) * \vec{F}_2(\theta,\varphi) d\Omega|}{\sqrt{\iint_{4\pi} |\vec{F}_1(\theta,\varphi)| d\Omega \iint_{4\pi} |\vec{F}_2(\theta,\varphi)| d\Omega}} \quad (1)$$

The results of ECC at 2.4 GHz are shown in TABLE 11. It lists ECC calculated by simulated S parameters, measured S parameters, and measured ECC in far field. As we can see, the results are all low in free space. When antenna is with cubic tissue model or wrist model, the results of d = 0.5 mm and d =2 mm are also low. The maximum value in TABLE 11 is just $1.368\times10^{-2}$, which is enough low to be used in MIMO applications.

### B. INFLUENCE OF BATTERY AND PCBA

Influences of the battery and PCBA (printed circuit board assembly) are studied. We replaced the foam board with a PEC and a lossy metal to mimic battery and PCBA, shown in the Fig. 12. The S parameters in free space are shown in Fig. 13. When the PCBA is not too close to the proposed antenna, the antenna can basically maintain the impedance matching. When the battery and PCBA are too large, the antenna needs to be redesigned. Gain and Radiation efficiency are listed in TABLE 12, which are not too much affected.

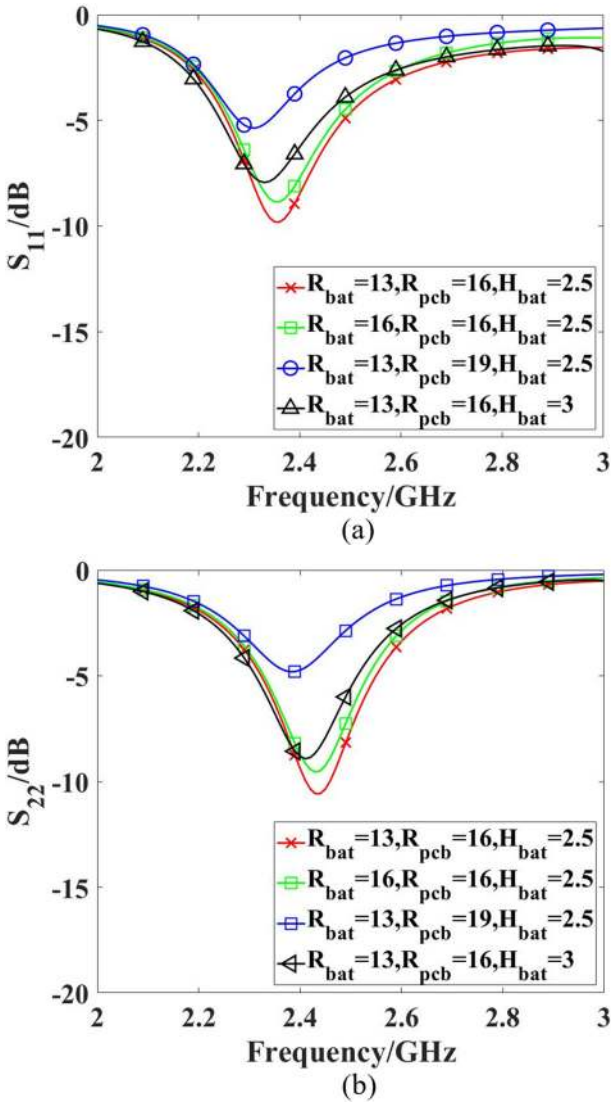


**FIGURE 13.** S parameters with battery and PCBA in free space. (a) $S_{11}$; (b) $S_{22}$. $H_{pcb}$ is 0.5mm. $R_{bat}$, $R_{pcb}$, $H_{bat}$ are in millimeters.

## V. CONCLUSION

A design of smartwatch integrated antenna with polarization diversity is proposed. The annular shape and the size of the proposed antenna make it easy to be integrated in the frame of the normal smartwatch. The polarization diversity is realized by exciting the two ports. The antenna is also analyzed with cubic tissue model and wrist model when the d is 2 mm and 0.5 mm respectively. According to the simulation and measurement results, the band ranges can cover 2.4 GHz WLAN band. The peak gains are higher than 2 dBi of both ports in free space and on body scenarios. The port isolation $S_{21}$ is lower than −13 dB from 2.4 GHz to 2.5GHz, and the cross-polarization is below −10 dB. The radiation efficiency is higher than 32% on cubic tissue model at 2.4 GHz, which is sufficient for smartwatch application, and it is even higher than 62% on wrist model. Besides, the 10-g SAR values and the 1-g SAR values calculated by HFSS and CST are analyzed, which are both less than the limitations set by FCC and ETSI. When the distance between the proposed antenna and human body scenario get closer, the gain and radiation efficiency will get lower and the SAR value will get higher, but the performances are also acceptable. The low ECC results show the proposed antenna can be applied on MIMO applications. The influence of the battery and PCBA on the S parameter is large, but it is not much affected on gain and efficiency of the proposed antenna. The results prove the proposed design of smartwatch integrated antenna is a suitable candidate for smartwatches.

## REFERENCES

[1] S. Yan, P. J. Soh, and G. A. E. Vandenbosch, "Compact all-textile dual-band antenna loaded with metamaterial-inspired structure," *IEEE Antennas Wireless Propag. Lett.*, vol. 14, pp. 1486–1489, 2015.

[2] S. Yan, G. A. E. Vandenbosch, and P. J. Soh, "Wearable dual-band composite right/left-handed waveguide textile antenna for WLAN applications," *Electron. Lett.*, vol. 50, no. 6, pp. 424–426, Mar. 2014.

[3] M. Haghi, R. Stoll, and K. Thurow, "Pervasive and personalized ambient parameters monitoring: A wearable, modular, and configurable watch," *IEEE Access*, vol. 7, pp. 20126–20133, 2019.

[4] S. Kwak, D. Sim, J. H. Kwon, and Y. J. Yonn, "Design of PIFA with metamaterials for body-SAR reduction in wearable applications," *IEEE Trans. Electromagn. Compat.*, vol. 59, no. 1, pp. 297–300, Feb. 2017.

[5] H. T. Chattha, Y. Huang, S. J. Boyes, and X. Zhu, "Polarization and pattern diversity-based dual-feed planar Inverted-F antenna," *IEEE Trans. Antennas Propag.*, vol. 60, no. 3, pp. 1532–1539, Mar. 2012.

[6] A. J. Khalilabadi and A. Zadehgol, "An ultra-thin triple-band smartwatch antenna with support of several wireless application bands," in *Proc. IEEE Int. Symp. Antennas Propag. USNC-URSI Radio Sci. Meeting*, Atlanta, GA, USA, Jul. 2019, pp. 1281–1282.

[7] C.-M. Cheng, W.-S. Chen, G.-Q. Lin, and H.-M. Chen, "Four antennas on smart watch for GPS/UMTS/ WLAN MIMO application," in *Proc. IEEE Int. Conf. Comput. Electromagn. (ICCEM)*, Kumamoto, Japan, Mar. 2017, pp. 346–348.

[8] Y. N. Jin and J. Choi, "Bandwidth enhanced compact dual-band smart watch antenna for WLAN 2.4/5.2GHz application," in *Proc. Int. Appl. Comput. Electromagn. Soc. Symp.*, Suzhou, China, 2017, pp. 1–2.

[9] H.-S. Huang, H.-L. Su, and S.-L. Chen, "Multiband antennas for GPS/GSM1800/bluetooth/Wi-Fi smart watch applications," in *Proc. IEEE Int. Conf. Comput. Electromagn. (ICCEM)*, Kumamoto, Japan, Mar. 2017, pp. 352–354.

[10] C.-Y. Chiu, S. Shen, and R. D. Murch, "Transparent dual-band antenna for smart watch applications," in *Proc. IEEE Int. Symp. Antennas Propag. USNC/URSI Nat. Radio Sci. Meeting*, San Diego, CA, USA, Jul. 2017, pp. 191–192.

[11] H. Zou, Y. Li, M. Peng, M. Wang, and G. Yang, "Triple-band loop antenna for 5G/WLAN unbroken-metal-rimmed smartwatch," in *Proc. IEEE Int. Symp. Antennas Propag. USNC/URSI Nat. Radio Sci. Meeting*, Boston, MA, USA, Jul. 2018, pp. 463–464.

[12] M. I. Ahmed and M. F. Ahmed, "Design of 5G smart watch with millimeter wave wearable antenna," in *Proc. 7th Int. Japan-Africa Conf. Electron., Commun., Comput. (JAC-ECC)*, Alexandria, Egypt, Dec. 2019, pp. 132–135.

[13] D. Wu and S. W. Cheung, "A cavity-backed annular slot antenna with high efficiency for smartwatches with metallic housing," *IEEE Trans. Antennas Propag.*, vol. 65, no. 7, pp. 3756–3761, Jul. 2017.

[14] C.-Y. Hong and S.-H. Yeh, "Cellular antenna design with metallic housing for wearable device," in *Proc. IEEE 5th Asia–Pacific Conf. Antennas Propag. (APCAP)*, Kaohsiung, Taiwan, Jul. 2016, pp. 419–420.

[15] S.-W. Su and Y.-T. Hsieh, "Integrated metal-frame antenna for smartwatch wearable device," *IEEE Trans. Antennas Propag.*, vol. 63, no. 7, pp. 3301–3305, Jul. 2015.

[16] W.-Z. Lee and W.-S. Chen, "An antenna design on metal frame of smart watch," in *Proc. Int. Workshop Electromagn., Appl. Student Innov. Competition (iWEM)*, Qingdao, China, Sep. 2019, pp. 1–2.

[17] Y. Jia, L. Liu, J. Hu, and L.-J. Xu, "Miniaturized wearable watch antenna for wristband applications," in *IEEE MTT-S Int. Microw. Symp. Dig.*, Nanjing, China, May 2019, pp. 1–3.

[18] G. Li, G. Gao, J. Bao, B. Yi, C. Song, and L.-A. Bian, "A watch strap antenna for the applications of wearable systems," *IEEE Access*, vol. 5, pp. 10332–10338, 2017.
[19] K. Zhao, Z. N. Ying, and S. L. He, "Antenna designs of smart watch for cellular communications by using metal belt," in *Proc. 9th Eur. Conf. Antennas Propag.*, Lisbon, Portugal, 2015, pp. 1–5.
[20] G. Li, G. Gao, W. Liu, J. Su, and Y. Bai, "An on-body watchband antenna for the applications of wearable systems," in *Proc. IEEE Int. Symp. Antennas Propag. USNC/URSI Nat. Radio Sci. Meeting*, San Diego, CA, USA, Jul. 2017, pp. 585–586.
[21] W. W. Li, J. H. Zhou, B. Zhang, and B. Q. You, "High isolation dual-port MIMO antenna," *Electron. Lett.*, vol. 49, no. 15, pp. 919–921, Jul. 2013.
[22] S. Yan, P. J. Soh, and G. A. E. Vandenbosch, "Dual-band textile MIMO antenna based on substrate-integrated waveguide (SIW) technology," *IEEE Trans. Antennas Propag.*, vol. 63, no. 11, pp. 4640–4647, Nov. 2015.
[23] S. Yan and G. A. E. Vandenbosch, "Wearable Antennas with Tripolarization Diversity for WBAN Communications," *Elec. Lett.*, vol. 52, no. 7, pp. 500–502, 2016.
[24] S. Yan and G. A. E. Vandenbosch, "Low-profile dual-band pattern diversity patch antenna based on composite Right/Left-handed transmission line," *IEEE Trans. Antennas Propag.*, vol. 65, no. 6, pp. 2808–2815, Jun. 2017.
[25] J. Zhang, S. Yan, and G. A. E. Vandenbosch, "Realization of dual-band pattern diversity with a CRLH-TL-Inspired reconfigurable metamaterial," *IEEE Trans. Antennas Propag.*, vol. 66, no. 10, pp. 5130–5138, Oct. 2018.
[26] C. B. Dietrich, K. Dietze, J. R. Nealy, and W. L. Stutzman, "Spacial, Polarization, and Pattern Diversity for Wireless Handheld Terminals," *IEEE Trans. Antennas Propag.*, vol. 49, no. 9, pp. 1271–1281, Sep. 2001.
[27] B. Wang, A. Zhang, and S. Yan, "A dual-port annular antenna with polarization diversity for smartwatches," in *Proc. Cross Strait Quad-Regional Radio Sci. Wireless Technol. Conf. (CSQRWC)*, Taiyuan, China, Jul. 2019, pp. 1–3.
[28] Y.-S. Chen and T.-Y. Ku, "A low-profile wearable antenna using a miniature high impedance surface for smartwatch applications," *IEEE Antennas Wireless Propag. Lett.*, vol. 15, pp. 1144–1147, 2016.
[29] *Electromagnetic Compatibility and Radio Spectrum Matters (ERM); Wideband Transmission Systems; Data Transmission Equipment operating in the 2.4GHz ISM band and Using Wideband Modulation Techniques; Harmonized EN Covering the Essential Requirements of Article 3.2 of the R&TTE Directive*, document 300 328 V1.8.1, Jul. 2012.
[30] P. J. Soh, G. Vandenbosch, F. H. Wee, A. van den Bosch, M. Martinez-Vazquez, and D. Schreurs, "Specific absorption rate (SAR) evaluation of textile antennas," *IEEE Antennas Propag. Mag.*, vol. 57, no. 2, pp. 229–240, Apr. 2015.
[31] S. Yan and G. A. E. Vandenbosch, "Design of wideband button antenna based on characteristic mode theory," *IEEE Trans. Biomed. Circuits Syst.*, vol. 12, no. 6, pp. 1383–1391, Dec. 2018.
[32] Y. Zheng, G. A. E. Vandenbosch, and S. Yan, "Low-profile broadband antenna with pattern diversity," *IEEE Antennas Wireless Propag. Lett.*, early access, May 21, 2020, doi: 10.1109/LAWP.2020.2996196.
[33] S. Blanch, J. Romeu, and I. Corbella, "Exact representation of antenna system diversity performance from input parameter description," *Electron. Lett.*, vol. 39, no. 9, pp. 705–707, May 2003.

**BUYUN WANG** received the bachelor's degree in information and telecommunication engineering from Xi'an Jiaotong University (XJTU), Xi'an, China, in 2019, where he is currently pursuing the master's degree with the Faculty of Electronics and Information Engineering, Institute of Electromagnetics and Information Technology.

His current research interests include wearable antennas and antenna diversity.

**SEN YAN** (Member, IEEE) received the bachelor's and master's degrees in information and telecommunication engineering from Xi'an Jiaotong University (XJTU), Xi'an, China, in 2007 and 2010, respectively, and the Ph.D. degree in electrical engineering from Katholieke Universiteit Leuven (KU Leuven), Leuven, Belgium, in 2015. From 2015 to 2017, he was a Postdoctoral Researcher with KU Leuven. He joined EPFL, Lausanne, Switzerland, in 2016. He was a Visiting Researcher with The University of Texas at Austin, Austin, TX, USA. Since 2017, he has been a Full Professor with XJTU. He has authored or coauthored 43 international journal articles and 40 conference contributions. His current research interests include metamaterials, metasurfaces, wearable devices, textile antennas, reconfigurable antennas, antenna diversity, and nano-antennas. He was successful in achieving the Postdoctoral Fellowship from KU Leuven and FWO, in 2015 and 2016, respectively. He received the Young Talent Support Plan from XJTU, in 2017, and the Young Scientist Award of the International Union of Radio Science (URSI), in 2019.